Dynamic PB2-E627K substitution of influenza H7N9 virus indicates the in vivo genetic tuning and rapid host adaptation

William J. Liu[a,b,1], Jun Li[c,1], Rongrong Zou[a,1], Jingcao Pan[c,1], Tao Jin[d,e], Liqiang Li[d], Peipei Liu[b], Yingze Zhao[b], Xinfen Yu[c], Haoqiu Wang[c], Guang Liu[d,e], Hui Jiang[d,e], Yuhai Bi[a,f,g], Lei Liu[a], Kwok-Yung Yuen[h], Yingxia Liu[a,2], and George F. Gao[a,b,f,g,2]

[a]Shenzhen Key Laboratory of Pathogen and Immunity, State Key Discipline of Infectious Diseases, Shenzhen Third People's Hospital, Second Hospital Affiliated to Southern University of Science and Technology, 518112 Shenzhen, China; [b]NHC Key Laboratory of Biosafety, National Institute for Viral Disease Control and Prevention, Chinese Center for Disease Control and Prevention, 102206 Beijing, China; [c]Hangzhou Center for Disease Control and Prevention, 310021 Hangzhou, China; [d]BGI-Shenzhen, 518083 Shenzhen, China; [e]China National GeneBank, BGI-Shenzhen, 518083 Shenzhen, China; [f]CAS Key Laboratory of Pathogenic Microbiology and Immunology, Institute of Microbiology, Chinese Academy of Sciences, 100101 Beijing, China; [g]Center for Influenza Research and Early-Warning, Chinese Academy of Sciences, 100101 Beijing, China; and [h]State Key Laboratory of Emerging Infectious Diseases and the HKU-Shenzhen Hospital, Li Ka Shing Faculty of Medicine, The University of Hong Kong, Pokfulam, Hong Kong Special Administrative Region, China

Edited by Peter Palese, Icahn School of Medicine at Mount Sinai, New York, NY, and approved August 5, 2020 (received for review July 6, 2020)

Avian-origin influenza viruses overcome the bottleneck of the interspecies barrier and infect humans through the evolution of variants toward more efficient replication in mammals. The dynamic adaptation of the genetic substitutions and the correlation with the virulence of avian-origin influenza virus in patients remain largely elusive. Here, based on the one-health approach, we retrieved the original virus-positive samples from patients with H7N9 and their surrounding poultry/environment. The specimens were directly deep sequenced, and the subsequent big data were integrated with the clinical manifestations. Unlike poultry/environment-derived samples with the consistent dominance of avian signature 627E of H7N9 polymerase basic protein 2 (PB2), patient specimens had diverse ratios of mammalian signature 627K, indicating the rapid dynamics of H7N9 adaptation in patients during the infection process. In contrast, both human- and poultry/environment-related viruses had constant dominance of avian signature PB2-701D. The intrahost dynamic adaptation was confirmed by the gradual replacement of 627E by 627K in H7N9 in the longitudinally collected specimens from one patient. These results suggest that host adaptation for better virus replication to new hosts, termed "genetic tuning," actually occurred in H7N9-infected patients in vivo. Notably, our findings also demonstrate the correlation between rapid host adaptation of H7N9 PB2-E627K and the fatal outcome and disease severity in humans. The feature of H7N9 genetic tuning in vivo and its correlation with the disease severity emphasize the importance of testing for the evolution of this avian-origin virus during the course of infection.

host adaptation | dynamic substitution | next-generation sequencing | H7N9 virus | PB2-627

In February 2013, avian influenza virus (AIV) A (H7N9) emerged in the Yangtze River delta region of eastern China and quickly spread to other adjacent provinces (1–3). To date, a total of 1,568 laboratory-confirmed cases of human infection by H7N9, with a case fatality rate (CFR) of ∼40%, have been reported to the World Health Organization (4). In addition to the original low-pathogenic viruses (5), in the winter of 2016, wave 5 of H7N9 appeared, with some highly pathogenic variants emerging (6). Most of the human cases had a history of direct exposure to or close contact with live poultry markets (LPMs) before disease onset, which implies a zoonotic origin of the virus (7–11), while only limited human-to-human transmission has been reported (12). However, the national surveillance on influenza in China reported the persistence of AIVs in the LPMs (13) and the sporadic human cases (14), indicating a continuous threat of the virus for public health (15–17) and even global biosecurity (18, 19).

Studies have reported key substitutions favorable for efficient H7N9 virus replication in mammalian hosts (20–23). While the AIVs usually contain Glu (E) at position 627 of polymerase basic protein 2 (PB2), mutation to Lys (K) is a well-recognized mammalian adaptation substitution at this position (22, 24). The single amino acid substitution at position 627 from Glu to Lys (E627K) in PB2 of avian-origin influenza virus was first revealed to be responsible for more efficient replication of the virus in mammalian cells (22). Later, the influence of PB2-627K on the outcome of challenged mice was confirmed in H5N1 (25). Studies on the pathogenicity of H7N9 in mammalian models, including mice (21, 23, 26), ferrets (20), and pigs (27), also indicated that PB2-627K is essential for the virulence of H7N9 viruses in mammals. However, studies on the longitudinal dynamics of the PB2-E627K substitution of the avian-origin virus in infected patients and its influence on disease severity are lacking.

Significance

Deep-sequencing of viral genomes based on original specimens from H7N9-infected patients and the surrounding poultry/environment has provided the first in-depth data on virus adaptation at the interface between poultry and humans. In contrast to the consistent dominance of 627E in poultry-derived H7N9, diverse but longitudinally changing ratios of the mammalian signature substitution PB2-E627K from patient specimens indicate a dynamic viral adaptation during infection, termed "genetic tuning" of avian influenza viruses in new hosts. Furthermore, the correlation between rapid host adaptation of H7N9 PB2-627 and the disease severity in patients is brought to light. Of note, under a one-health vision, our study provides direct big data evidence that "genetic tuning" of PB2-E627K is associated with H7N9 pathogenicity during human infection.

Author contributions: W.J.L., J.P., and G.F.G. designed research; J.L., R.Z., Y.Z., and X.Y. performed research; W.J.L., J.L., R.Z., T.J., L. Li, P.L., H.W., G.L., H.J., Y.B., and L. Liu analyzed data; and W.J.L., K.-Y.Y., Y.L., and G.F.G. wrote the paper.

Competing interest statement: T.J., L. Li., G.L., and H.J. were employees of BGI-Shenzhen during the project.

This article is a PNAS Direct Submission.

[1]W.J.L., J.L., R.Z., and J.P. contributed equally to this work.

[2]To whom correspondence may be addressed. Email: yingxialiu@hotmail.com or gaofu@chinacdc.cn.

This article contains supporting information online at https://www.pnas.org/lookup/suppl/doi:10.1073/pnas.2013267117/-/DCSupplemental.

First published September 1, 2020.

Mammal infection models have shown dynamic substitution of E627K occurring during acute infection with avian-origin influenza viruses (e.g., H5N1, H10N8) with the avian signature 627E (28, 29). This dynamic substituting process has also been previously confirmed in human infections of highly pathogenic AIVs (HPAIVs) of the H5N1 and H7N7 subtypes (30, 31). H7N9 viruses also show intrahost and interhost adaptive substitution at PB2-627 during transmission and infection in numerous mammalian models, including mice, ferrets, and pigs (21, 27, 32, 33). However, the adaptive dynamics of PB2-E627K in H7N9 infected patients and the surrounding poultry/environment under the vision of one health has not yet been investigated.

In the present work, deep sequencing of the H7N9 virus from humans has provided in-depth data on virus adaptation in vivo together with intrahost single nucleotide variation (iSNV). Evolution modes for key mammal-adaptive mutations, including PB2-E627K, were found to differ between LPM- and patient-derived samples, indicating the dynamics of the "genetic tuning" of the H7N9 virus in adapting to the mammalian host. Furthermore, the correlation between in vivo rapid host adaptation of PB2-627 in H7N9 and disease severity was also investigated. These findings provide beneficial data for understanding the influenza–host interaction and the adaptation of H7N9 in humans.

Results

Coexisting Peaks for Codons of Lys and Glu in the PB2-627 Position. The H7N9 PB2 segment covering position 627 in respiratory samples from 39 H7N9 patients (Hangzhou, $n = 22$; Shenzhen, $n = 17$) were analyzed (Table 1). The first standard Sanger sequencing data of the 20 samples available in Hangzhou showed that the majority ($n = 15$) of the human samples had the H7N9 bearing solely Lys in PB2-627, while two others had only Glu in this position. Interestingly, mixed peaks of A and G as the first nucleotide of the codon encoding amino acids at PB2-627 were observed with traces of PB2 genes from three samples in Hangzhou City (samples 3, 254, and 327) (Fig. 1). The intensive peak of A at the first nucleotide of the codon AAG for Lys (627K) mixing with a recessive peak for the G resulting in the codon GAG for Glu (627E) occurred in Hangzhou/3 and Hangzhou/254, while a weak signal of A arose in Hangzhou/327 with a coexisting dominant G, implying ongoing dynamic substitutions.

Differential Patterns of E627K Substitution in the H7N9 Viruses from Patients and LPMs. Deep sequencing was next introduced to further investigate the H7N9 PB2 segment covering position 627 in the respiratory samples from H7N9 patients and also the samples collected from the surrounding poultry and environment. To elucidate the substitution of 627E by 627K in all the specimens, we used an index, the ratio of K/E (i.e., sequence depths of 627K to 627E), to compare the relative abundances of 627K and 627E in the specimens. All the human samples had diverse 627K reads and 627E reads in the PB2 segment but with divergent dominance among the patients (Fig. 2*A*). Seven patients in Shenzhen had a Val at 627 (Last section of *Results*). The K/E ratio ranged from 1,510:1 to 1:2,000, consistent with the results of mixed 627K and 627E from the Sanger DNA analyzer. The detected ratios of these residues to the entire depth of PB2-627 (depth of target residue/whole depth of the position) from human samples are diverse, especially for 627K (0 to 0.9829) and 627E (0 to 0.9654) (Fig. 2*B*). Along with Lys and Glu, other residues, including Arg, Asn, Thr, Met, Gly, Val, Gln, His, Asp, Ala, and Pro, were detected in PB2-627 of human samples in the deep sequencing analyses (Fig. 2*B*).

For comparison, 38 avian or environmental samples from the patient-contacting LPMs were also analyzed. In contrast to the human samples, the poultry/environment-derived samples showed a different pattern for the coexisting amino acids in PB2-627. Viruses carrying 627E were dominant species in all the poultry/environment-derived samples, while viruses carrying 627K were not detectable in 12 (31.6%) samples under high sequencing depths (>1,000) (Fig. 2*A*). This substitution pattern was detected in different poultry/environment samples with a constant ratio in the whole depths; for example, the ratios of 627E in the total depths were >0.99 in all poultry/environment-derived samples, while the ratios for 627G ranged from 0.001 to 0.01, higher than those for other substitutions (Fig. 2*C*).

The different intrahost virus substitution patterns, especially Lys and Glu appearing in PB2-627 of the H7N9 virus from patient specimens and poultry/environment samples, indicates a dynamic interspecies adaptation of H7N9 virus occurring in humans.

Different D701N Substitution Patterns Compared with E627K. It has been demonstrated that, in addition to E627K, the substitution of D701N in PB2 is also responsible for the higher virulence of AIV in mammals (26, 34). To elucidate the substitution of 701D by 701N in all the specimens, we used the index ratio of N/D (sequence depths of 701N to 701D) to characterize the relative abundance of 701N compared with 701D in the specimens. The deep-sequencing analyses of H7N9 viruses showed that avian signature 701D dominated in all the patient and poultry/environment specimens (Fig. 3*A*), although the 701D ratio was higher in the poultry/environment specimens ($P = 0.0001$) (*SI Appendix*, Fig. S1). Several patients in Shenzhen had a dominant 701E (Last section of *Results*). Under the current sequencing depths (>1,000), human signature Asn was not detectable in 17.9% (7/39) of the human samples and in 34.2% (13/38) of poultry/environment-related H7N9 viruses. The occurrence patterns of other amino acids at PB2-701 of H7N9 were similar between the human and poultry/environment specimens, including similar iSNVs coding for Gly, Ala, Val, Tyr, and His (Fig. 3 *B* and *C*), while human viruses coded for additional Lys, Arg, and Gln. The ratios of Asn detected in the whole sequencing depths of PB2-701 remained similar between human- and poultry/environment-derived H7N9 viruses, with medians of 0.065% and 0.044%, respectively (Fig. 3*B* and *C*). Notably, 701G appeared in most human specimens (except M1/2015) and all poultry/environment specimens, and the detected ratio in the sequencing depth remained at a consistent level (Fig. 3*B* and *C*). This may indicate a complementary role of 701G in the function of PB2 in both human- and poultry/environment-related H7N9.

Dynamic Adaptation or In Vivo Genetic Tuning of H7N9 PB2 in Humans. Six longitudinally collected specimens from one patient (ID 14–49) enabled the observation of the dynamic substitution of the avian signature Glu to human signature Lys at PB2-627 of H7N9. The patient's infection was laboratory-confirmed on day 5 after the development of fever, and the patient died on day 16. We also used the index ratio of K/E (sequence depths of 627K to 627E) to elucidate the dynamic substitution of 627E by 627K in the patient. From day 5 to day 13 after disease onset, the ratio of Lys to Glu at PB2-627 increased from 4.8 (depths: 16,792/34,86) to 118.4 (depths: 24,636/208) in the throat swab samples (Fig. 4). On day 5, throat swab and sputum specimens from the same patient were collected and analyzed for the PB2-627 substitution. Interestingly, the ratio of Lys/Glu at PB2-627 of the virus from throat swab (4.8; depths: 16,792/3,486) was higher than that from sputum (1.2; depths: 13,670/11,125). Meanwhile, avian signature substitute Asp dominated the position PB2-701 compared with the mammalian signature substitute Asn in this position. From day 5 to day 13 after disease onset, the ratio of Asn/Asp in position PB2-701 in the patient's throat swab fluctuated between 0.001 and 0.0002, which may reflect a less essential role of substitution 701N for the H7N9 virus adaptation in humans.

Rapid Adaptation of PB2-E627K Predicts a Fatal Outcome. Although the dynamic adaptation of the human signature substitution was

Table 1. Information on specimens from H7N9-infected patients

Patient ID	Specimen	Age, y	Sex	Date of onset	Date of specimen collection	Outcome	City
1	Nasal lavage fluids	39	M	2013/3/7	2013/3/24	Died	Hangzhou
2	Pharyngeal swab	67	M	2013/3/20	2013/4/1	Recovered	Hangzhou
3	Pharyngeal swab	79	M	2013/3/29	2013/4/8	Recovered	Hangzhou
169	Pharyngeal swab	66	M	2013/4/8	2013/4/11	Died	Hangzhou
173	Pharyngeal swab	74	M	2013/4/7	2013/4/11	Recovered	Hangzhou
174	Pharyngeal swab	37	M	2013/4/6	2013/4/12	Recovered	Hangzhou
175	Pharyngeal swab	65	M	2013/4/3	2013/4/12	Recovered	Hangzhou
208	Pharyngeal swab	73	F	2013/4/10	2013/4/14	Died	Hangzhou
211	Pharyngeal swab	62	F	2013/3/29	2013/4/14	Died	Hangzhou
219	Pharyngeal swab	54	M	2013/4/11	2013/4/15	Recovered	Hangzhou
232	Sputum	58	F	2013/4/11	2013/4/15	Recovered	Hangzhou
250	Pharyngeal swab	37	F	2013/4/11	2013/4/16	Recovered	Hangzhou
253	Pharyngeal swab	74	M	2013/4/8	2013/4/17	Recovered	Hangzhou
254	Nasal lavage fluids	86	M	2013/4/12	2013/4/17	Died	Hangzhou
259	Pharyngeal swab	69	M	2013/4/11	2013/4/17	Died	Hangzhou
327	Pharyngeal swab	56	M	2013/4/11	2013/4/19	Recovered	Hangzhou
332	Pharyngeal swab	37	M	2013/3/30	2013/4/19	Recovered	Hangzhou
347	Pharyngeal swab	58	M	2013/4/16	2013/4/20	Recovered	Hangzhou
351	Pharyngeal swab	79	F	2013/4/13	2013/4/20	Recovered	Hangzhou
353	Sputum	54	F	2013/4/16	2013/4/20	Recovered	Hangzhou
14–40	Pharyngeal swab	40	M	2014/1/18	2014/1/24	Died	Hangzhou
14–49*	Pharyngeal swab	78	M	2014/1/24	2014/1/29	Died	Hangzhou
S4/2014	Pharyngeal swab	55	M	2014/1/6	2014/1/14	Recovered	Shenzhen
S8/2014	Nasal	76	M	2014/1/10	2014/1/20	Recovered	Shenzhen
S7/2014	Sputum	39	F	2014/1/17	2014/1/21	Recovered	Shenzhen
S10/2014	Pharyngeal swab	82	M	2013/12/26	2014/1/23	Recovered	Shenzhen
M18/2014	Sputum	57	M	2014/3/6	2014/3/13	Recovered	Shenzhen
D22/2014	Pharyngeal swab	48	M	2014/3/16	2014/3/23	Died	Shenzhen
M1/2015	Nasal	6	F	2015/1/2	2015/1/4	Recovered	Shenzhen
D2/2015	Pharyngeal swab	42	M	2015/1/5	2015/1/11	Died	Shenzhen
D3/2015	Pharyngeal swab	57	F	2015/1/7	2015/1/12	Died	Shenzhen
D5/2015	Pharyngeal swab	67	M	2015/1/10	2015/1/16	Died	Shenzhen
S7/2015	Pharyngeal swab	74	F	2015/1/18	2015/1/26	Recovered	Shenzhen
M8/2015	Pharyngeal swab	21	M	2015/1/21	2015/1/28	Recovered	Shenzhen
S9/2015	Pharyngeal swab	77	M	2015/1/24	2015/2/3	Recovered	Shenzhen
S10/2015	Pharyngeal swab	51	M	2015/1/27	2015/2/4	Recovered	Shenzhen
S11/2015	Pharyngeal swab	52	M	2015/2/2	2015/2/7	Recovered	Shenzhen
M4/2015	Sputum	57	F	2015/2/10	2015/2/12	Recovered	Shenzhen
M5/2015	Pharyngeal swab	41	M	2015/1/9	2015/1/12	Recovered	Shenzhen

*Patient 14–49 also had one sputum sample and four additional swab samples, as shown in Fig. 4.

observed in longitudinally collected specimens from patient 14–49, we did not find a linear correlation between the 627K substitution (ratio of Lys depths/whole depths in PB2-627) of H7N9 PB2 and days after disease onset in the aggregate analyses that included other patients (Fig. 5*A*). This may reflect diverse adaptation processes of the H7N9 viruses in different patients during the acute phase of the infection, as shown in Fig. 2.

The next question is whether the diverse patterns of the PB2-627 adaptation among the patients are correlated with disease severity and outcome. To reveal the emerging velocity of target amino acid at the PB2-627 site of the virus, we analyzed the K ratio in whole depths/days (emerging of 627K depth per day). Our analysis of the correlation between the adaptation of H7N9 PB2-E627K and the patient outcomes revealed a rapid E627K substitution in the patients who died (Fig. 5*B*). The rapidly adapted H7N9 virus may have a higher virus replication capacity, contributing to greater virulence in the fatal cases. We further analyzed the relationship of the 627K with the oxygenation index (PaO_2/FiO_2), an important prognostic indicator, inversely correlated with the ventilation function of the lung in the influenza virus-infected patients. The PaO_2/FiO_2 on the first day of hospitalization is negatively correlated with the "genetic tuning" indexes, including 627K among whole sequencing depths, 627K ratio in whole depths per day, K/E ratio, and K/E substitution per day (Fig. 5*C* and *SI Appendix*, Figs. S2*A* and S3*A* and *C*). Meanwhile, the time to the normalization of PaO_2/FiO_2 is positively correlated with the 627K (Fig. 5*D* and *SI Appendix*, Figs. S2*B* and S3*B* and *D*).

Emerging PB2-627V in H7N9 Viruses from Seven Patients and the Clinical Impact. Among the patients in Shenzhen City are seven patients whose H7N9 viruses all possessed a dominant Val at the PB2-627 position on the day of hospitalization (Fig. 2*B*). The depth ratios of all of the other amino acids appearing at this site were <0.1. For PB2-701, 701E emerged with depth ratio >0.3 in six patients and 0.053 in one patient (Fig. 3*B*). Interestingly, we found that the emerging iSNVs 701E and 627V are linked to each other, as shown by the close correlation of the depth ratios in different patients (Spearman's r = 0.79, $P = 0.0001$) (*SI Appendix*, Fig. S4). Meanwhile, positively charged amino acids Arg and Lys also take certain ratios at the PB2-701 position, with 0.03–0.13 for Arg and 0.01–0.17 for Lys.

In the patients from Shenzhen City, the emerging 627V had an inverse correlation with disease severity (Fig. 5). The PaO_2/FiO_2 on the first day of hospitalization was positively correlated with

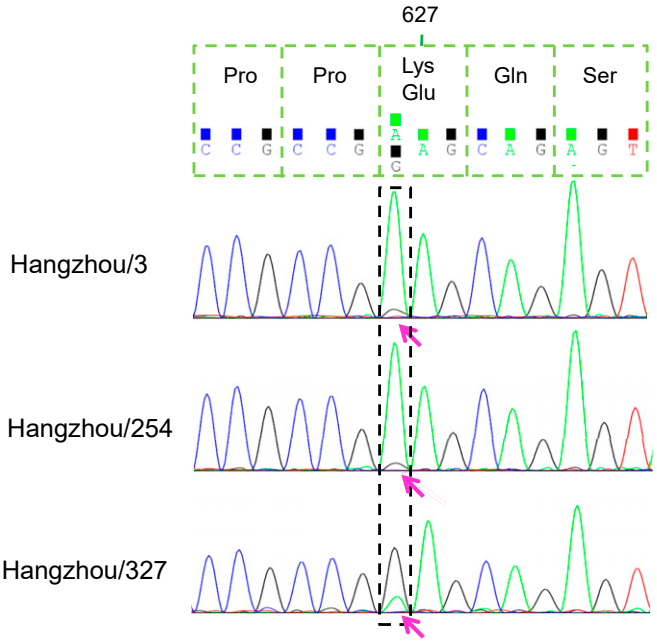

Fig. 1. The coexistence of 627K and 627E of H7N9 PB2 in human specimens based on a chromatogram of Sanger sequencing. The dashed boxes show the nonsynonymous substitutions. The dominant peak of A, which is the first nucleotide of the codon AAG for 627K, and the recessive peak of G for the codon GAG of 627E are observed in H7N9 viruses from two patients (ID 3 and 254) and vice versa in H7N9 from one patient (ID 327). The purple arrowheads point to the peaks for G and A in the PB2 gene, acting as the first nucleotides of the codons for coexistent 627E and 627K, respectively.

the 627V substitution-related indices, such as 627V ratio in the whole depths/days (Fig. 5*E*) and 627V ratios in the whole depths (*SI Appendix*, Fig. S2*C*). The time to normalization of PaO_2/FiO_2 in the patients was not related to these indices (Fig. 5*F* and *SI Appendix*, Fig. S2*D*).

Discussion

In terms of a one-health approach, the deep sequencing (i.e., next-generation sequencing) of original viral-positive samples from avian influenza patients and their surrounding poultry/environment provides a direct demonstration of in vivo host adaptation. The coexistence and the divergent ratios of the mammalian signature amino acids and avian signature amino acids in the key sites of H7N9 viruses (e.g., PB2-627) from patients imply the dynamic occurrence of viral "genetic tuning" in human during the course of infection in vivo. Interestingly, virus adaptation can predict the disease severity in patients infected by H7N9, which may be contributed by the distinct virulence and pathogenicity of the H7N9 virus with different mammalian signature substitutions in the patients (35, 36). Meanwhile, the rapid interspecies adaptation of the influenza viruses may also impact the development of seasonal influenza vaccine, as indicated in the adaptation of H3N2 vaccine strain in embryonated eggs (37).

Although the mechanisms by which the PB2-627 substitutions impact the pathogenesis of influenza viruses are not yet determined, three independent theories have been proposed. First, key mammalian signature residues, including 627K, that form the basic face of PB2 can directly regulate polymerase activity and then influence viral replication (38). The human 627K mutant polymerase is catalytically more active than the avian 627E polymerase at lower temperatures, which enables the viruses to preferentially replicate at the low temperatures in the human respiratory tract (39, 40). Second, unlike PA and PB1, the other two components in the RNA polymerase complex of the influenza virus, PB2 is independently imported into the nucleus before polymerase reconstitution by interaction of the PB2 C terminus with cytoplasmic importins (41). An increase in charged surface residues, such as E627K, during host adaptation may increase the rate of association of PB2 to importins (42, 43). Third, mammalian-adaptive 627K may influence PB2 function through different host factors (44, 45). Long et al. (46) reported that ANP32A represents an essential host partner co-opted to support influenza virus replication by adapting the viral polymerase with host-specific substitutions at PB2-627. DEAD box RNA helicase DDX17/p72 protein differentially regulates H5N1 polymerase according to avian- or mammalian-adaptive PB2 genotypes (44). Another host factor, RIG-I, directly inhibits the onset of infection by destabilizing nucleocapsids through binding at positions related to PB2-627 polymorphisms of influenza viruses (45). Strains with the mammalian-adapted polymerase subunit PB2-627K are more RIG-I–resistant than those with avian-adapted PB2-627E, due to the different strengths of polymerase binding to their nucleocapsids. In addition, host immune responses induced by the virus strains with different PB2-627 substitutions may also contribute to the distinct pathogenicity of the viruses in humans (23, 47). Forero et al. (48) found that PB2 of 1918 H1N1 also inhibits activation of the Wnt/β-catenin signaling pathway, which enhances detrimental inflammatory responses, coupled with the loss of the regeneration and repair functions coordinated by Wnt.

In this study, we found a marked adaptation of 627V in the PB2 in H7N9 viruses from seven patients in Shenzhen, indicating a strong selection pressure in these patients. E627V is reportedly associated with H5N1 adaptation in MDCK cells (49) and can also enhance H9N2 polymerase activity in human cells and mouse virulence (50). These studies imply that 627V supposedly produces some effect to increase polymerase activity compared with 627E in a range of AIVs. Considering the hydrophobic features of Val compared with the positively charged Lys and negatively charged Glu, PB2-627V may produce an intermediate effect between PB2-627E and PB2-627K to maintain PB2 function in mammals; this merits further investigation. However, it has been demonstrated that PB2-627V can be transmitted and stably maintained in both avian and mammalian species (33). Based on these mechanisms, the impact of PB2-627 substitutions on the adaptation of influenza viruses may lead to different patient outcomes, as shown in this study.

Similar to PB2-627, substitutions at PB2-701 have also been implicated in expanding the host range of avian subtype influenza viruses to mice and humans (34). D701N appears to enhance the binding of PB2 to importin and to correspondingly increase PB2 levels in the nucleus in mammalian cells, but not avian cells (41). In the mammalian H7N9 virus infection model, Asn at position 701 in PB2 is also considered essential for greater polymerase activity and improved viral replication in mammalian cells and enhanced virulence in mice (21). The D701N adaptation could readily occur during transmission of the virus among ferrets (20). Asn in PB2-701 also has been reported in human-derived H7N9 virus (10). However, no dominant 701N substitutions were observed in any of the specimens in our study. The adaptation of D701N during the natural infection of H7N9 in humans may be less essential for virus replication.

In addition to E627K and D701N, previous studies also identified a series of other mammalian adaptation substitutions (e.g., Q591K on the basic surface PB2 of influenza virus) that may have compensatory functions in the activity of polymerase complexes of influenza viruses (32, 51, 52). Furthermore, PB2-K526R is found in human isolates of H7N9 (84%), H5N1 (74%), and H3N2 (99.7%). Polymerase complexes containing PB2-526R derived from H7N9 and H5N1 exhibit increased polymerase

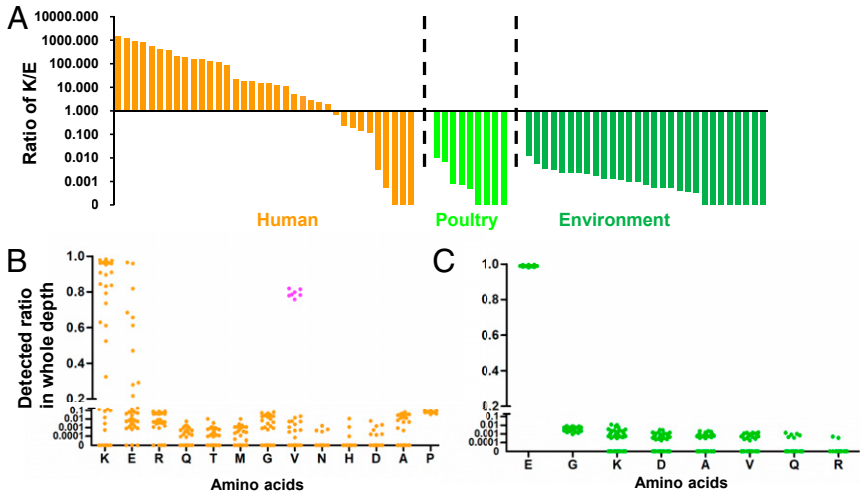

Fig. 2. Different patterns for substitutions at PB2-627 of H7N9 in patient and surrounding poultry/environment samples. (*A*) K/E ratios at PB2-627 of H7N9 in different samples from H7N9 patients ($n = 36$; samples S10/2014, M1/2015, and M5/2015 with neither K nor E reads are not shown), poultry ($n = 9$), and environment ($n = 29$) where the patients may be exposed before the illness onset. (*B* and *C*) Detected ratios of different amino acids at PB2-627 within the total sequencing depths of the H7N9 viruses from patients (*B*; $n = 39$) and poultry/environment (*C*; $n = 38$). Detected ratio in the whole depth = detected depth of target amino acid/sequencing depth. The amino acids in H7N9 viruses from patients and poultry/environment are shown in orange and green, respectively. The ratios for amino acid V in the seven patients (M18/2014, S10/2014, D22/2014, M1/2015, M5/2015, M8/2015, and D3/2015) with a dominant PB2-627V virus are shown in purple.

activity and enhanced viral transcription and replication in cells. H7N9 viruses carrying both 526R and 627K replicate more efficiently in mammalian (but not avian) cells and in mouse lung tissues and cause greater body weight loss and mortality in infected mice. Arai et al. (50) showed that PB2-E627V/E543D/A655V/K526R mutations act cooperatively to produce the high polymerase activity of PB2 and efficient replication of the H9N2 virus in human cells and to increase replication and pathogenicity in mice in vivo. PB2-K526R has been shown to interact with nuclear export protein, which enhances virus replication, particularly in combination with 627K (53).

The next key question is the compensatory role of these different mutation sites in PB2. Previous studies have implied distinct roles of D701N and K526R when combined with E627K. Although Zhu et al. (20) reported multiple mutations of E627K/D701N in ferrets infected with H7N9 viruses, D701N has not been detected together with PB2-E627K among field AIV strains with a few exceptions, implying little synergistic effect with PB2-E627K. In contrast, K526R/E627K multiple mutations occurred in the field and had strong orchestral effects on mammalian adaptation of H7N9 and H9N2 viruses (50, 53). Thus, the deep sequencing used in this study provided valuable big data to demonstrate the genetic tuning of H7N9 and gave insight into the compensatory roles and interdependency of these substitutions during the adaptation process of H7N9. We found a linked and simultaneous adaptation of 701E with 627V in the PB2 of

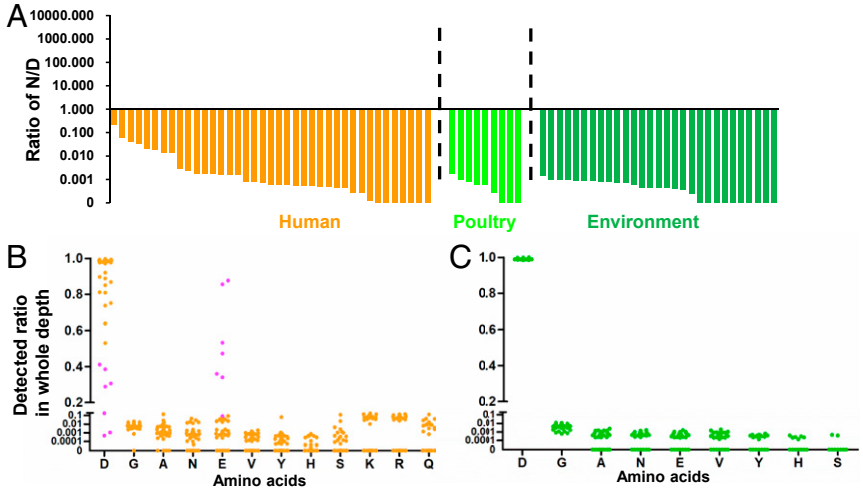

Fig. 3. Patterns of substitutions at PB2-701 of H7N9 in patient and surrounding poultry/environmental samples. (*A*) N/D ratios at PB2 site 701 of H7N9 in patients ($n = 39$), poultry ($n = 9$), and surrounding environment ($n = 29$). (*B* and *C*) Detected ratios of different amino acids at PB2-701 within the total sequencing depths of the H7N9 viruses from patients (*B*; $n = 39$) and poultry/environment (*C*; $n = 38$). The detected ratio in the whole depth is calculated as in Fig. 2*C*. The amino acids in H7N9 viruses from patients (orange) and poultry/environment (green) are shown in the same order. The ratios for amino acid 701E and the corresponding 701D in the seven patients (M18/2014, S10/2014, D22/2014, M1/2015, M5/2015, M8/2015, and D3/2015) with a dominant PB2-627V virus are shown in purple.

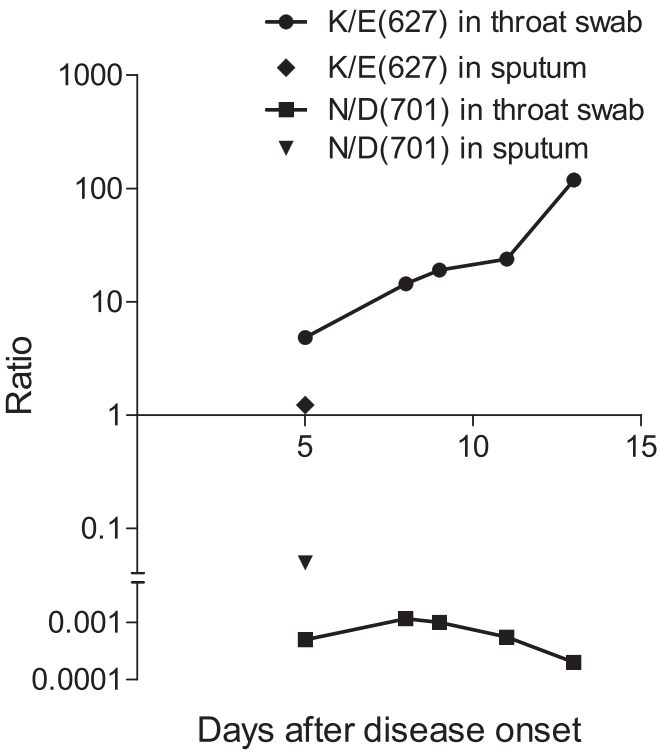

Fig. 4. Dynamic adaptation for the substitutions in PB2-627 and -701 of H7N9 in longitudinal specimens from one patient. Shown are the K/E ratios at site 627 and N/D ratios at site 701 of H7N9 PB2 in longitudinally collected throat swab and sputum samples from one H7N9-infected patient (ID 14–49) during the acute infection. The throat swab samples were collected on days 5, 8, 9, 11, and 13. The sputum sample from the same patient was also available on day 5.

H7N9 viruses from seven patients in Shenzhen, possibly indicating that D701E coemerges on the same alleles carrying E627V in the virus quasi-species. Determining how the negatively charged residue 701E compensates for the polymerase activity of PB2 carrying 627V requires further structural exploration (54).

In addition to the key sites in the influenza virus PB2 protein, some HA amino acids also play critical roles in host adaptation. In a previous study, after 10 passages in mice to generate mouse-adapted H7N9 influenza viruses, the H7N9 virulence in mice and virus titer in MDCK cells were significantly increased. Amino acid changes revealed amino acid substitutions also located in HA (H3 numbering: R220G, L226S, and G279R) in addition to PB2-E627K (55). Kawaoka et al. (56) also demonstrated that the enhanced viral replication and virulence in mice infected by influenza virus encoding the Venus fluorescent protein are conferred primarily by the PB2 and HA mutations. The adaptation patterns of E627K coupled with substitutions in these positions and their association with the outcome of the patients require further exploration.

Our deep-sequencing data demonstrate the different patterns of substitutions in H7N9 viruses from patient and poultry/environmental samples under a one health vision, and suggest a disease severity-related dynamic adaptation of the virus in humans. These findings are helpful for the understanding of the in vivo evolution of H7N9 in humans. Our study strongly supports the notion that viral genetic tuning is essential for human infection of AIVs.

Materials and Methods

Specimen Collection and Laboratory Confirmation of H7N9 Infection. Between 2013 and 2014, respiratory tract specimens (throat swab or nasopharyngeal aspirate samples) from hospitalized patients with symptoms of fever, cough, and severe acute respiratory illness in Hangzhou City, Zhejiang Province, China were collected in specimen tube with viral-transport medium (Hank's buffer). Between 2013 and 2015, related samples were collected from patients in Shenzhen City, Guangzhou Province, China. All of the samples were submitted to test for influenza viruses in laboratory within 24 h under similar protocol.

The diagnosis of human H7N9 infections was confirmed if nucleic acids of the H7N9 viruses were detected in the respiratory specimens by real-time PCR assay. The assay was conducted with an ABI 7500 PCR system (Thermo Fisher Scientific) with RNA extracted from the samples using the RNeasy Mini Kit (Qiagen). Two cohorts comprising 22 H7N9 patients from Hangzhou City and another 17 H7N9 patients from Shenzhen City were enrolled (Table 1).

Once human H7N9 infection was confirmed, standardized epidemiologic investigations were carried out. Retrospective information on demographic characteristics, possible routes of virus acquisition, clinical symptoms, and illness onset and progression was collected.

In addition, a total of 355 samples from local LPMs in Hangzhou that were epidemiologically linked to human cases were collected to test for H7N9 viruses. These samples consisted of cloacal and throat swabs of chickens and ducks, smear specimens from surface of poultry cages and poultry feces, and others. These LPMs were visited by the patients with H7N9 infection before the onset of illness, were located near patient's residences, or both. A total of 38 samples from patient-contacted LPMs were confirmed as H7N9-positive (*SI Appendix*, Table S1).

Nested RT-PCR and Deep Sequencing of Genetic Regions Covering PB2-627 and 701. Viral RNA was extracted from specimens of H7N9-infected patients and samples from patient-contacted LPMs using the RNeasy Mini Kit (Qiagen). Standard RT-PCR was performed with primers specific for full-length PB2 of the influenza A virus (The primer Uni12 for reverse transcription, and primers Ba-PB2-1 and Ba-PB2-2341R for PCR) (57) using the PrimeScript II First-Strand cDNA Synthesis Kit and Ex-Taq HS (TaKaRa). Then a nested PCR was conducted with the primers for the 1,239-bp PB2 segment (PB2-3F-1054: 5′-gaa gtg ctc aca ggc aac ctc at-3′; PB2-4R-2292: 5′-ccg aat cct ttt ggt cgc tg-3′), covering the codons of PB2 residues 627 and 701, using the foregoing RT-PCR products as templates. The segments in the PCR products of human specimens in Hangzhou were first analyzed using an ABI 3730 automatic DNA analyzer (Thermo Fisher Scientific). Subsequently, the 1,239-bp PCR products were fragmented by sonication in a Covaris LE220 focused ultrasonicator and then processed by end repair, A-tailing, adapter ligation, DNA size selection, PCR amplification, and product purification according to the manufacturer's instructions (Illumina). The DNA libraries with an insert size of 300 bp were sequenced by 150-bp paired-end sequencing on an Illumina MiSeq Personal Sequencer.

Data Assembly and Analysis. Deep-sequencing reads were cleaned by filtering out low-quality reads (eight reads with quality <66), duplication, poly-Ns (with eight Ns) and adaptor-contaminated (with >15 bp matched to the adapter sequence) reads. We used BWA version 0.7.3a (58) and samtools version 0.1.19 (59) to perform assembly based on the reference PB2 segment sequence of A/Hangzhou/1/2013 (3). We used SOAP software (60) to map high-quality reads to the final assemblies and acquired the depth and nucleotide polymorphism of each nucleotide site. Based on the depth and nucleotide polymorphism at each position, the ratios of different amino acids were calculated in the PB2-627 and -701 sites from the short reads bearing the consecutive 627 and 701 codons, respectively, using an in-house PERL script.

We used a series of indices to quantitatively elucidate the genetic tuning of the virus and the substitution of 627E by 627K or 701D by 701N in PB2. The ratio of K/E (sequence depths of 627K to 627E) and ratio of N/D (sequence depths of 701N to 701D) were used to characterize the relative abundance of 627K compared with 627E in the specimens and to quantify the substitution of E627K and D701N in the viruses (Figs. 2*A*, 3*A*, and 4). To reveal the emerging of target amino acids (i.e., Lys at the site PB2-627 of the virus), we used the K ratio in whole depths (i.e., detected ratios of the target residue to the whole depths of PB2-627) and the K ratio in whole depths/days (emerging 627K depths per day) (Figs. 2*B* and *C*, 3 *B* and *C*, and 5).

Statistics. Student's *t* test was performed with SPSS 16.0 for Windows. A *P* value <0.05 derived from a two-tailed test of all analyses was considered statistically significant. Linear correlation was analyzed using Spearman's rank correlation coefficient.

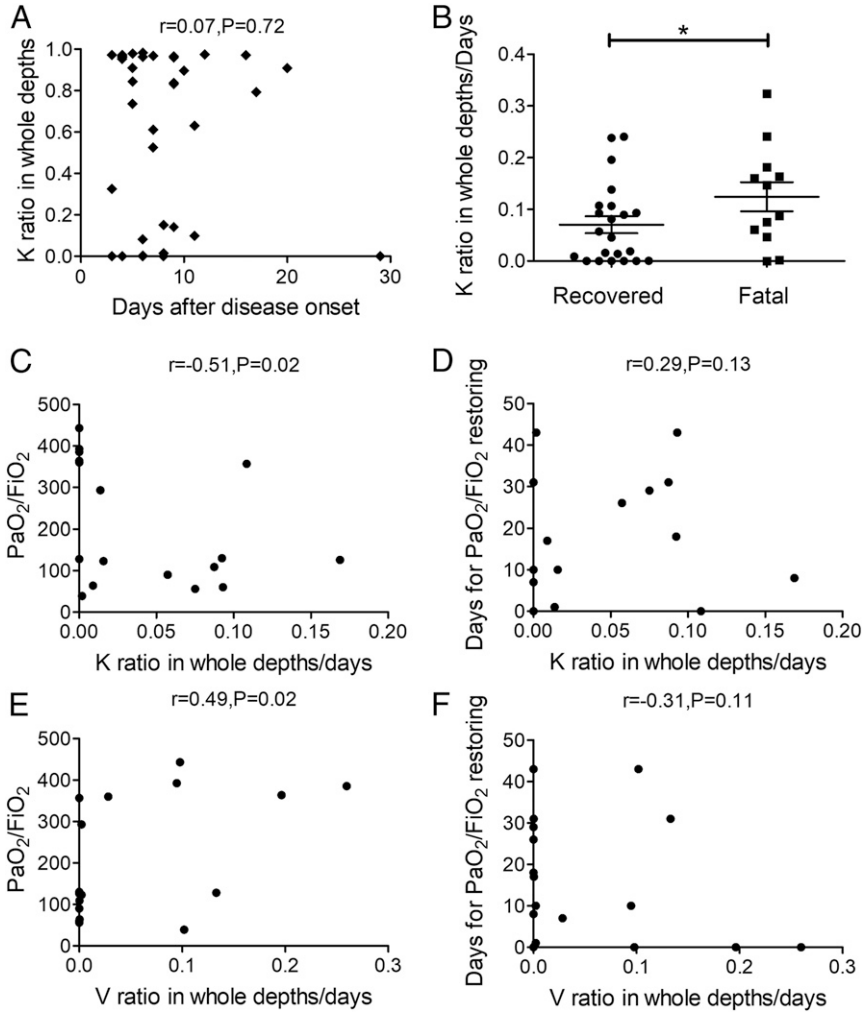

Fig. 5. Adaptation of PB2-627 associates with disease severity in H7N9 patients. (*A*) Linear regression analysis of Lys ratios (depths of Lys/whole depths of position 627) at PB2-627 of H7N9 with the corresponding days after disease onset ($n = 39$). Each plot represents an individual patient. (*B*) Early adaptation of E627K (indicated by Lys ratios/days after disease onset) in the upper respiratory tract of deceased patients compared with recovered patients ($n = 34$). Data for the five sputum samples from patients 232, 353, M4/2015, M18/2014, and S7/2014 are not shown. (*C*) Correlation of PaO_2/FiO_2 measured on the first day of hospitalization with the 627K ratio among whole depths per day since disease onset. Data of the Shenzhen patients ($n = 17$) are shown. (*D*) Correlation of PaO_2/FiO_2 restoration time of patients and the 627K ratio among whole depths per day since disease onset ($n = 17$). (*E*) Correlation of the PaO_2/FiO_2 on the first day of hospitalization with the 627V ratio among whole depths per day since disease onset ($n = 17$). (*F*) Correlation of the normalization time of PaO_2/FiO_2 and the 627V ratio among whole depths/days since disease onset ($n = 17$). Data from the Hangzhou patients without available clinical information are not shown. $*P < 0.05$, Student's *t* test. Spearman's rank correlation coefficient analysis was performed for linear correlation.

Study Approval. This study was approved by the Ethics Review Committees of the National Institute for Viral Disease Control and Prevention, Chinese Center for Disease Control and Prevention, and Shenzhen Third People's Hospital. The study was conducted in accordance with the principles of the Declaration of Helsinki and the standards of good clinical practice (as defined by the International Conference on Harmonization). Informed written consent for the studies performed on their samples and the publication of their cases were provided by patients, the mothers of young children, or immediate relatives of deceased patients.

Data Availability. All study data are included in the main text and *SI Appendix*.

ACKNOWLEDGMENTS. We thank Drs. Hui Wang and Haixia Xiao for their helpful suggestions. This work was supported by the Hangzhou Key Medicine Discipline Fund sponsored by the Hangzhou government (20150733Q45), the Shenzhen Science and Technology Research and Development Projects (JCYJ20150402111430617 and JCYJ20151029151932602), and the Key Specialized Fund for New Infectious Diseases in Shenzhen City (201161). W.J.L. is supported by the Excellent Young Scientist Program of the National Natural Science Foundation of China (NSFC) (81822040). K.-Y.Y. was partially supported by the High-Level Hospital Summit Program in Guangdong. G.F.G. is a leading principal investigator of the (NSFC) Innovative Research Group (81621091).

1. G. F. Gao, From "A"IV to "Z"IKV: Attacks from emerging and re-emerging pathogens. *Cell* **172**, 1157–1159 (2018).
2. R. Gao *et al*., Human infection with a novel avian-origin influenza A (H7N9) virus. *N. Engl. J. Med.* **368**, 1888–1897 (2013).
3. J. Li *et al*., Environmental connections of novel avian-origin H7N9 influenza virus infection and virus adaptation to the human. *Sci. China Life Sci.* **56**, 485–492 (2013).
4. World Health Organization, https://www.who.int/influenza/human_animal_interface/influenza_h7n9/Risk_Assessment/en/. Accessed 20 August 2020.
5. J. Liu *et al*., H7N9: A low pathogenic avian influenza A virus infecting humans. *Curr. Opin. Virol.* **5**, 91–97 (2014).
6. X. Wang *et al*., Epidemiology of avian influenza A H7N9 virus in human beings across five epidemics in mainland China, 2013-17: An epidemiological study of laboratory-confirmed case series. *Lancet Infect. Dis.* **17**, 822–832 (2017).
7. G. F. Gao, Influenza and the live poultry trade. *Science* **344**, 235 (2014).
8. Y. Wu, G. F. Gao, Compiling of comprehensive data of human infections with novel influenza A (H7N9) virus. *Front. Med.* **7**, 275–276 (2013).

9. C. J. Bao *et al*., Live-animal markets and influenza A (H7N9) virus infection. *N. Engl. J. Med.* **368**, 2337–2339 (2013).
10. Y. Chen *et al*., Human infections with the emerging avian influenza A H7N9 virus from wet market poultry: Clinical analysis and characterisation of viral genome. *Lancet* **381**, 1916–1925 (2013).
11. D. Liu *et al*., Origin and diversity of novel avian influenza A H7N9 viruses causing human infection: Phylogenetic, structural, and coalescent analyses. *Lancet* **381**, 1926–1932 (2013).
12. H. Chen *et al*., Nosocomial co-transmission of avian influenza A(H7N9) and A(H1N1) pdm09 viruses between 2 patients with hematologic disorders. *Emerg. Infect. Dis.* **22**, 598–607 (2016).
13. C. Quan *et al*., Avian influenza A viruses among occupationally exposed populations, China, 2014-2016. *Emerg. Infect. Dis.* **25**, 2215–2225 (2019).
14. W. Shi *et al*., Co-circulation and persistence of multiple A/H3N2 influenza variants in China. *Emerg. Microbes Infect.* **8**, 1157–1167 (2019).
15. C. Quan *et al*., Genomic characterizations of H4 subtype avian influenza viruses from live poultry markets in Sichuan province of China, 2014-2015. *Sci. China Life Sci.* **61**, 1123–1126 (2018).
16. Y. Bi *et al*., Genesis, Evolution and prevalence of H5N6 avian influenza viruses in China. *Cell Host Microbe* **20**, 810–821 (2016).
17. Y. Bi *et al*., Clinical and immunological characteristics of human infections with H5N6 avian influenza virus. *Clin. Infect. Dis.* **68**, 1100–1109 (2019).
18. G. F. Gao, China's outreach to the world: public health goes global. *China CDC Week* **1**, 1–2 (2019).
19. G. Wu, Laboratory biosafety in China: Past, present, and future. *Biosaf Health* **1**, 56–58 (2019).
20. W. Zhu *et al*., Dual E627K and D701N mutations in the PB2 protein of A(H7N9) influenza virus increased its virulence in mammalian models. *Sci. Rep.* **5**, 14170 (2015).
21. S. Yamayoshi *et al*., Amino acids substitutions in the PB2 protein of H7N9 influenza A viruses are important for virulence in mammalian hosts. *Sci. Rep.* **5**, 8039 (2015).
22. E. K. Subbarao, W. London, B. R. Murphy, A single amino acid in the PB2 gene of influenza A virus is a determinant of host range. *J. Virol.* **67**, 1761–1764 (1993).
23. Y. Bi *et al*., Assessment of the internal genes of influenza A (H7N9) virus contributing to high pathogenicity in mice. *J. Virol.* **89**, 2–13 (2015).
24. N. Naffakh, P. Massin, N. Escriou, B. Crescenzo-Chaigne, S. van der Werf, Genetic analysis of the compatibility between polymerase proteins from human and avian strains of influenza A viruses. *J. Gen. Virol.* **81**, 1283–1291 (2000).
25. M. Hatta, P. Gao, P. Halfmann, Y. Kawaoka, Molecular basis for high virulence of Hong Kong H5N1 influenza A viruses. *Science* **293**, 1840–1842 (2001).
26. C. K. Mok *et al*., Amino acid substitutions in polymerase basic protein 2 gene contribute to the pathogenicity of the novel A/H7N9 influenza virus in mammalian hosts. *J. Virol.* **88**, 3568–3576 (2014).
27. Q. Liu *et al*., Analysis of recombinant H7N9 wild-type and mutant viruses in pigs shows that the Q226L mutation in HA is important for transmission. *J. Virol.* **88**, 8153–8165 (2014).
28. K. Mei *et al*., Deep sequencing reveals the viral adaptation process of environment-derived H10N8 in mice. *Infect. Genet. Evol.* **37**, 8–13 (2016).
29. J. Y. Min *et al*., Mammalian adaptation in the PB2 gene of avian H5N1 influenza virus. *J. Virol.* **87**, 10884–10888 (2013).
30. M. Jonges *et al*., Emergence of the virulence-associated PB2 E627K substitution in a fatal human case of highly pathogenic avian influenza virus A(H7N7) infection as determined by Illumina ultra-deep sequencing. *J. Virol.* **88**, 1694–1702 (2014).
31. Q. M. Le, Y. Sakai-Tagawa, M. Ozawa, M. Ito, Y. Kawaoka, Selection of H5N1 influenza virus PB2 during replication in humans. *J. Virol.* **83**, 5278–5281 (2009).
32. L. Xu *et al*., Novel avian-origin human influenza A(H7N9) can be transmitted between ferrets via respiratory droplets. *J. Infect. Dis.* **209**, 551–556 (2014).
33. G. S. Luk *et al*., Transmission of H7N9 influenza viruses with a polymorphism at PB2 residue 627 in chickens and ferrets. *J. Virol.* **89**, 9939–9951 (2015).
34. J. Steel, A. C. Lowen, S. Mubareka, P. Palese, Transmission of influenza virus in a mammalian host is increased by PB2 amino acids 627K or 627E/701N. *PLoS Pathog.* **5**, e1000252 (2009).
35. X. Ding, J. Luo, L. Quan, A. Wu, T. Jiang, Evolutionary genotypes of influenza A (H7N9) viruses over five epidemic waves in China. *Infect. Genet. Evol.* **55**, 269–276 (2017).
36. S. Su *et al*., Epidemiology, evolution, and pathogenesis of H7N9 influenza viruses in five epidemic waves since 2013 in China. *Trends Microbiol.* **25**, 713–728 (2017).
37. L. Yang *et al*., Mutations associated with egg adaptation of influenza A(H1N1)pdm09 virus in laboratory-based surveillance in China, 2009–2016. *Biosafety Heal.* **1**, 41–45 (2019).
38. J. Kirui, M. D. Bucci, D. S. Poole, A. Mehle, Conserved features of the PB2 627 domain impact influenza virus polymerase function and replication. *J. Virol.* **88**, 5977–5986 (2014).
39. P. Massin, S. van der Werf, N. Naffakh, Residue 627 of PB2 is a determinant of cold sensitivity in RNA replication of avian influenza viruses. *J. Virol.* **75**, 5398–5404 (2001).
40. S. Aggarwal, S. Dewhurst, T. Takimoto, B. Kim, Biochemical impact of the host adaptation-associated PB2 E627K mutation on the temperature-dependent RNA synthesis kinetics of influenza A virus polymerase complex. *J. Biol. Chem.* **286**, 34504–34513 (2011).
41. F. Tarendeau *et al*., Structure and nuclear import function of the C-terminal domain of influenza virus polymerase PB2 subunit. *Nat. Struct. Mol. Biol.* **14**, 229–233 (2007).
42. S. Boivin, D. J. Hart, Interaction of the influenza A virus polymerase PB2 C-terminal region with importin alpha isoforms provides insights into host adaptation and polymerase assembly. *J. Biol. Chem.* **286**, 10439–10448 (2011).
43. E. Delaforge *et al*., Large-scale conformational dynamics control H5N1 influenza polymerase PB2 binding to importin alpha. *J. Am. Chem. Soc.* **137**, 15122–15134 (2015).
44. E. Bortz *et al*., Host- and strain-specific regulation of influenza virus polymerase activity by interacting cellular proteins. *MBio* **2**, e00151-11 (2011).
45. M. Weber *et al*., Influenza virus adaptation PB2-627K modulates nucleocapsid inhibition by the pathogen sensor RIG-I. *Cell Host Microbe* **17**, 309–319 (2015).
46. J. S. Long *et al*., Species difference in ANP32A underlies influenza A virus polymerase host restriction. *Nature* **529**, 101–104 (2016).
47. J. L. Fornek *et al*., A single amino acid substitution in a polymerase protein of an H5N1 influenza virus is associated with systemic infection and impaired T-cell activation in mice. *J. Virol.* **83**, 11102–11115 (2009).
48. A. Forero *et al*., The 1918 influenza virus PB2 protein enhances virulence through the disruption of inflammatory and Wnt-mediated signaling in mice. *J. Virol.* **90**, 2240–2253 (2015).
49. A. S. Taft *et al*., Identification of mammalian-adapting mutations in the polymerase complex of an avian H5N1 influenza virus. *Nat. Commun.* **6**, 7491 (2015).
50. Y. Arai *et al*., PB2 mutations arising during H9N2 influenza evolution in the Middle East confer enhanced replication and growth in mammals. *PLoS Pathog.* **15**, e1007919 (2019).
51. A. Mehle, J. A. Doudna, Adaptive strategies of the influenza virus polymerase for replication in humans. *Proc. Natl. Acad. Sci. U.S.A.* **106**, 21312–21316 (2009).
52. S. Yamada *et al*., Biological and structural characterization of a host-adapting amino acid in influenza virus. *PLoS Pathog.* **6**, e1001034 (2010).
53. W. Song *et al*., The K526R substitution in viral protein PB2 enhances the effects of E627K on influenza virus replication. *Nat. Commun.* **5**, 5509 (2014).
54. W. Zhang *et al*., Crystal structure of the swine-origin A (H1N1)-2009 influenza A virus hemagglutinin (HA) reveals similar antigenicity to that of the 1918 pandemic virus. *Protein Cell* **1**, 459–467 (2010).
55. J. Qin *et al*., Multiple amino acid substitutions involved in the adaption of three avian-origin H7N9 influenza viruses in mice. *Virol. J.* **16**, 3 (2019).
56. H. Katsura *et al*., Amino acid changes in PB2 and HA affect the growth of a recombinant influenza virus expressing a fluorescent reporter protein. *Sci. Rep.* **6**, 19933 (2016).
57. E. Hoffmann, J. Stech, Y. Guan, R. G. Webster, D. R. Perez, Universal primer set for the full-length amplification of all influenza A viruses. *Arch. Virol.* **146**, 2275–2289 (2001).
58. H. Li, R. Durbin, Fast and accurate short read alignment with Burrows-Wheeler transform. *Bioinformatics* **25**, 1754–1760 (2009).
59. H. Li *et al*.; 1000 Genome Project Data Processing Subgroup, The sequence alignment/map format and SAMtools. *Bioinformatics* **25**, 2078–2079 (2009).
60. R. Li *et al*., De novo assembly of human genomes with massively parallel short read sequencing. *Genome Res.* **20**, 265–272 (2010).